Available online at www.sciencedirect.com
SCIENCE DIRECT®
Journal of Sound and Vibration 291 (2006) 107–131
JOURNAL OF SOUND AND VIBRATION
www.elsevier.com/locate/jsvi

Digital holography and Karhunen–Loève decomposition for the modal analysis of two-dimensional vibrating structures

Umberto Iemma*, Luigi Morino, Matteo Diez

Dipartimento di Ingegneria Meccanica ed Industriale, Università Roma Tre, Via della Vasca Navale 79, 00146 Rome, Italy

Received 15 March 2004; received in revised form 8 March 2005; accepted 31 May 2005
Available online 24 August 2005

Abstract

The aim of this paper is to present the basic theory and preliminary applications of a newly developed formulation for the modal analysis of two-dimensional vibrating structures. This is based on the statistical processing of the data extracted from holographic shots of the vibrating object. Specifically, the elastic displacement field is obtained through digital processing of two series of holographic shots (generated by laser beams in quadrature), and then the Karhunen–Loève decomposition (KLD) technique is used to extract, from the data, base functions that are optimal in the sense of maximum content of energy (as understood in signal theory). The coupling of these two well-assessed techniques represents the main novelty of the present work and yields an experimental methodology characterized by several interesting features. First, the use of holographic images as data source provides a non-invasive technique that allows for an accurate analysis of certain phenomena (such as aeroelastic and acoustoelastic problems) for which instrumentation of the experimental models represents a critical issue. Also, it yields simultaneous three-dimensional information on the whole object domain. Moreover, the KLD provides empirical base functions which coincide, in theory, with the fundamental modes of vibration and requires a relatively inexpensive experimental rig to capture high-frequency modes; these in turn are related to the resolution of the digitized holographic shot, and not to the time-sampling rate. In the present work, the optical holographic process is simulated through a dedicated, in-house developed, computer program. The displacement field has been evaluated analytically for simple two-dimensional structures, such as thin homogeneous rectangular plates and membranes. Preliminary numerical results reveal that the KLD base functions obtained with the numerical simulation coincide, within plotting accuracy, with the exact eigenmodes of the structure. In the simulation of the process, attention is paid to the treatment of the

*Corresponding author.
E-mail addresses: u.iemma@uniroma3.it (U. Iemma), l.morino@uniroma3.it (L. Morino), m.diez@uniroma3.it (M. Diez).

0022-460X/$ - see front matter
doi:10.1016/j.jsv.2005.05.029

measurement noise, always present in real acquisitions. It is shown that the statistical nature of the KLD ensures that the results are not affected by uncorrelated noise with spacially uniform amplitude, even for a very poor signal-to-noise ratio.

1. Introduction

In the present work, a newly developed, non-invasive and accurate method for modal identification in the dynamics of two-dimensional vibrating structures is presented. The method is based on the coupling between digital holography and Karhunen–Loève theory. The data extracted from a set of holographic shots of the vibrating structure are processed according to Karhunen–Loève decomposition (KLD) in order to obtain the modal shapes. Indeed, the coupling of these two techniques, which represents the main novelty of the present work, provides an experimental methodology characterized by very attractive features discussed below. The emphasis is on the use of the KLD to extract the natural modes of vibration and on the advantages of using holographic images as empirical data source.

The KLD is a statistical method for finding a base that covers the optimal distribution of energy in the dynamics of a continuum. This method initially appeared in the signal processing literature, where it was presented by Hotelling [1] in 1933 as the principal component analysis (PCA). The theory behind the method was taken again and studied in depth by Kosambi [2] in 1943, Loève [3] in 1945 and Karhunen [4] in 1946. Since it was applied by Lumley [5] in 1967 to uncover coherent structures in turbulent flows, it has become a standard tool in turbulence studies [6], where it is also known as the proper orthogonal decomposition (POD). More recently, the theory proposed by Karhunen and Loève caught the attention of the structural dynamicists and it is now emerging as a powerful tool also in structural dynamics and vibration. A physical interpretation of the use of the KLD in vibrations studies has been shown by Feeny and Kappagantu [7], Feeny [8,9], Kerschen and Golinval [10] and Wolter et al. [11] and Wolter and Sampaio [12].

The method consists in constructing a time-averaged spatial autocorrelation tensor from the elastic displacement field of the structure. Its spectral analysis produces a basis, as a set of orthonormal eigenfunctions (eigenvectors, in the numerical approach) and the corresponding set of eigenvalues, which represent the energy content of each mode. A very appealing property of the KLD is represented by its optimality: for a given truncation order n, the projection of the data set on the first n eigenfunctions produced by the expansion "captures" more energy, on average, than a projection on the first n functions of any other orthonormal basis. Therefore, the basis given by the KLD is optimal in the sense of maximum energy content [6].

In the present work, the KLD is applied to identify the modal shapes of two-dimensional structures. It is shown that for an undamped and unforced two-dimensional structure with constant mass per unit area, the decomposition gives the eigenfunctions of the structural operator.

In the numerical applications presented at the end of the present work, attention is paid to the treatment of the experimental noise, always present in actual data acquisitions. It will be shown how the KLD acts as a filter for uncorrelated noise with spacially uniform amplitude, even for very poor signal-to-noise ratios. It is worth noting that the statistical nature of the Karhunen–Loève technique yields an additional feature, very attractive from the experimental

point of view: the capability to capture high-frequency modes depends on the resolution of the digitized holograms, and not on the time sampling rate. This is essentially due to the time-averaging of the autocorrelation tensor, and makes this method particularly suitable for coupling to optical data acquisitions, resulting in an experimental setup much less expensive than those currently used.

Holographic interferometry is an extension of interferometric measurement techniques and it may be used to generate a spatial image of objects deflection. Holographic techniques have shown their capability to give accurate measurements of displacement vectors of a structure and, among the traditional interferometric methods, they have a major advantage: holography permits storing a wavefront for reconstruction at later time (see Section 3). Holographic methods have been successfully applied by Erf [13] in non-destructive testing since 1974 and they are now used wherever deformations and changes in shape of objects have to be evaluated with interferometric accuracy. Furthermore, holographic interferometry has been found very useful in other area of applications such as aerodynamics, heat transfer, medical and dental research [14]. For the objective of vibrational analysis of elastic structures, the use of holographic images as a data source has two major advantages: (i) the optical data acquisition is a non-invasive technique which drastically reduce the errors due to the instrumentation; (ii) the data acquisition covers the whole object domain so that it is possible to store information for a large number of points.

The technique can detect both out- and in-plane deformations of surfaces and has been widely applied to study static loading problems (e.g., Refs. [15,16]). Its use in vibration problems has been successfully used in the past years to observe single-frequency motion (e.g., Ref. [17]). In the present work, a method to measure out-of-plane displacements of a two-dimensional structure is presented. The present technique may be used to observe arbitrary time-dependent phenomena and it has been here used to study a multi-frequency motion.

The recent growth of digital technologies has permitted the use of digital devices in holography, so that the optical field intensity can be stored in a CCD array and read out by a computer system. In this paper, the use of high-resolution and high-speed digital devices in holographic measurements of displacement field of a structure is shown. Nevertheless, as already mentioned, the use of the KLD makes it possible to use low speed recording devices, even for the analysis of high-frequency motions, with a significant reduction of the effort required.

In Section 2, the general theory underlying the KLD is briefly presented, with emphasis on its application to quasi-periodic dynamical systems. The relationship existing between the empirical base functions and the fundamental modes of vibration of the structure is addressed as well. Section 3 deals with the use of holographic interferometry for the evaluation of the elastic displacements of vibrating two-dimensional objects, whereas in Section 4 preliminary numerical results are presented, by means of a computer simulation of the vibratory phenomenon and its optical acquisition. In Section 5, attention is paid to the simulation of the experimental noise, in order to investigate the impact on the eigenfunctions extracted, for various signal-to-noise ratios.

2. Karhunen–Loève decomposition

The aim of the methodology introduced by Karhunen and Loève is to provide an *optimal* basis for the representation of an ensemble of (scalar) fields $w(\mathbf{x})$. In our case, $\mathbf{x} \in \mathscr{S}$, being $\mathscr{S}$ the

surface of a two-dimensional structure. The KLD basis is given by those functions φ which maximize, on average, the square-scalar-product of w onto φ, suitably normalized (for details, see Ref. [6]). This condition implies that, for a given truncation order n, the first n KLD base functions capture, on average, more energy than any other orthonormal basis (a complete proof of this property is given in Ref. [6]). It may be shown that the optimal base functions are the solution of the integral equation

$$\mathscr{L}_R\varphi(\mathbf{x}) \coloneqq \int_{\mathscr{S}} R(\mathbf{x},\mathbf{y})\varphi(\mathbf{y})\,\mathrm{d}\mathbf{y} = \lambda\varphi(\mathbf{x}), \tag{1}$$

where for real scalar fields, $R(\mathbf{x},\mathbf{y}) = \langle w(\mathbf{x})\, w(\mathbf{y})\rangle$ is the time-averaged autocorrelation function ($\langle\cdot\rangle$ is the time-averaging operator). In other words, the KLD basis is formed by the eigensolutions of $\mathscr{L}_R$, and the field w may be decomposed in the linear combination. It may be shown that the operator $\mathscr{L}_R$ is selfadjoint and compact (since $R(\mathbf{x},\mathbf{y})$ is symmetric and bounded). Hence, its eigenfunctions form a complete set of orthogonal functions,[1] such that the displacement field $w(\mathbf{x},t)$ may be expressed as

$$w(\mathbf{x}) = \sum_{j=1}^{\infty} a_j\varphi_j(\mathbf{x}). \tag{2}$$

In our application, the scalar field $w(\mathbf{x})$ is the elastic displacement of a vibrating two-dimensional structure, and it may be easily shown that the empirical eigenvalue λ_j represents the value of the energy content of the mode φ_j.[2] It follows that, for a given n, the subspace spanned by the φ_j ($j = 1,\ldots,n$) maximizes, on average, the energy content of Eq. (2), truncated to the order n.

2.1. The KLD for undamped unforced system with constant mass per unit area

Let the KLD data set be a representation of a time-dependent displacement field of a vibrating two-dimensional structure with constant mass per unit area (e.g., a plate or a membrane).[3] The out-of-plane displacements w over the structure domain $\mathscr{S}$ solve the equation of the dynamics for the undamped and unforced system, $\ddot{w} + \mathscr{L}w = 0$ (the constant mass per unit area is included in $\mathscr{L}$)

$$w(\mathbf{x},t) = \sum_{k=1}^{\infty} \alpha_k(t)\phi_k(\mathbf{x}), \quad \mathbf{x}\in\mathscr{S}, \tag{3}$$

with ϕ_k solutions of $\mathscr{L}\phi_k = \mu_k\phi_k$ and

$$\alpha_k(t) = a_k\,\cos(\omega_k t + \chi_k), \tag{4}$$

[1] Specifically, the functions solutions of the eigenproblem integral equation (Eq. (1)) are orthonormal (for details, see Refs. [6,18]).

[2] A proof for a scalar field representing a turbulent velocity field is given in Ref. [19]. In that case, the empirical eigenvalues are twice the kinetic energy of the associated empirical eigenfunction.

[3] The demonstration that follows is closely related to those given in Refs. [7,10,11].

where $\omega_k = \sqrt{\mu_k}$, $a_k \in \Re$, $\chi_k \in \Re$ (determined by initial conditions). The averaged autocorrelation function of the real field $w(\mathbf{x}, t)$ is, by definition,

$$\begin{aligned} R(\mathbf{x}, \mathbf{y}) &:= \frac{1}{T}\int_0^T w(\mathbf{x}, t) w(\mathbf{y}, t)\, \mathrm{d}t \\ &= \frac{1}{T}\int_0^T \left[\sum_{i=1}^{\infty} \alpha_i(t)\phi_i(\mathbf{x})\right]\left[\sum_{k=1}^{\infty} \alpha_k(t)\phi_k(\mathbf{y})\right] \mathrm{d}t \\ &= \sum_{i=1}^{\infty}\sum_{k=1}^{\infty}\left[\frac{1}{T}\int_0^T \alpha_i(t)\alpha_k(t)\, \mathrm{d}t\right]\phi_i(\mathbf{x})\phi_k(\mathbf{y}) \\ &= \sum_{i=1}^{\infty}\sum_{k=1}^{\infty} c_{ik}\phi_i(\mathbf{x})\phi_k(\mathbf{y}), \end{aligned} \tag{5}$$

where

$$c_{ik} := \frac{1}{T}\int_0^T \alpha_i(t)\alpha_k(t)\, \mathrm{d}t. \tag{6}$$

Under the condition $\omega_i \neq \omega_k$ for $i \neq k$, it may be shown (see Appendix A) that, as $T \to \infty$ the matrix $\mathbf{C} := [c_{ik}]$ becomes diagonal

$$\lim_{T\to\infty} c_{ik} = \frac{a_k^2}{2}\,\delta_{ik}. \tag{7}$$

Hence, for $T \to \infty$, the time-averaged autocorrelation function may be written, in the diagonal form, as

$$R(\mathbf{x}, \mathbf{y}) = \frac{1}{2}\sum_{k=1}^{\infty} a_k^2 \phi_k(\mathbf{x})\phi_k(\mathbf{y}). \tag{8}$$

This equation implies that $\varphi(\mathbf{x}) = \phi(\mathbf{x})$, whereas

$$\lambda_j = \tfrac{1}{2}a_j^2. \tag{9}$$

Indeed, it is easy to verify that these are solutions of Eq. (1), with R given by Eq. (8). In addition, Mercer's theorem (for details, see Ref. [18]) ensures the uniqueness of the diagonal representation of R in terms of eigenvalues and eigenfunctions of the operator $\mathscr{L}_R$, so that we are allowed to state that those KLD eigenfunctions that correspond to non-zero KLD eigenvalues are fundamental modes of vibration of the structure.

Note that Eq. (9) confirms that the eigenvalues are related to the energy content of the corresponding modes. Thus, the above-mentioned optimality of the KLD ensures that, for a given truncation order n, the subspace spanned by the first n eigenfunctions of the structural operator (fundamental modes) maximizes, on average, the energy content of the signal.

3. Elastic displacements from optical field

In this section, we briefly outline the basic optics analytical tools relevant to the understanding of the present methodology. In this application, we consider a thin deformable plate, lying in the xy-plane, capable of out-of-plane deformation. When a laser beam hits the object at rest, the reflected optical field may be considered as the effects of a sources distribution $V_r(x, y, z_o)$ on the object plane $z = z_o$. On the other hand, indicating with $w(x, y)$ the out-of-plane displacement due to a (static) deformation, the complex representation of the relationship between the distribution $V_r(x, y, z_o)$ and that emanating from the deformed plate is

$$V(x, y, z_o) = V_r(x, y, z_o)\mathrm{e}^{\imath k_z w(x,y,t)}, \tag{10}$$

where k_z is the wavenumber of the coherent light in the z-direction. For a vibrating object, Eq. (10) becomes

$$V(x, y, z_o, t) = V_r(x, y, z_o)\mathrm{e}^{\imath k_z w(x,y,t)}. \tag{11}$$

The complete information about the two fields $V_r(x, y)$ and $V(x, y)$ may be recorded on a suitable device, such as a photographic film or a digital CCD, using a real-time holographic technique (for details, see Refs. [14,17]). To this aim, the recording device is illuminated by two different laser beams coming, respectively, from the object (object beam $O(x, y, z, t)$ produced by the sources given by Eq. (10) or Eq. (11), see Fig. 1), and from a known source (reference beam $R(x, y, z)$, see

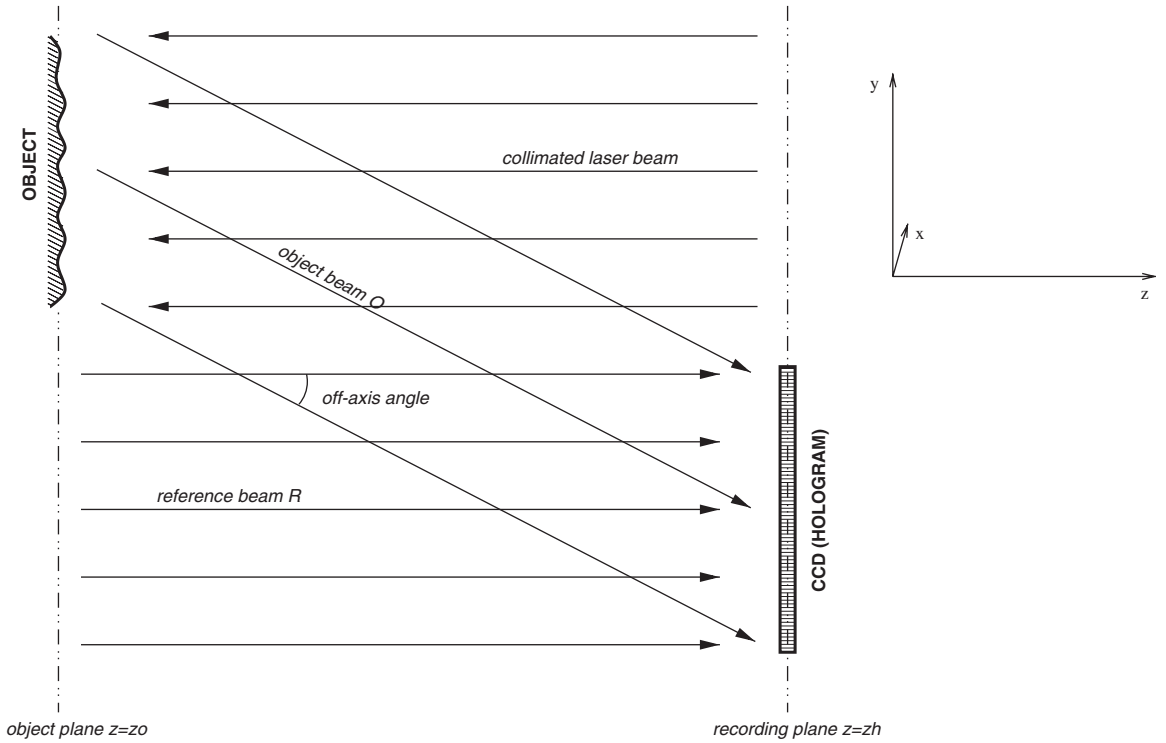

Fig. 1. Scheme of the holographic optical setup.

again Fig. 1). The resulting optical field intensity (i.e., the quantity the recording medium is sensible to) may be expressed by the superposition, on the holographic plane $z = z_h$, of the two incoming beams

$$\begin{aligned} I_h(x,y,t) &= |R(x,y,z_h) + O(x,y,z_h,t)|^2 \\ &= |R(x,y,z_h)|^2 + |O(x,y,z_h,t)|^2 \\ &\quad + R(x,y,z_h)O^*(x,y,z_h,t) + R^*(x,y,z_h)O(x,y,z_h,t), \end{aligned} \tag{12}$$

where $z = z_h$ is the recording plane and $*$ indicates the complex conjugate. To reconstruct completely the displacement field from the recorded data, we need to know the complex optical field. To accomplish this, it is convenient to record two different simultaneous holograms, using two reference beams in quadrature

$$R_0(x,y,z_h) = A, \quad R_{\pi/2}(x,y,z_h) = A\mathrm{e}^{\imath\pi/2}, \tag{13}$$

where A is a real constant. The corresponding intensities on the holographic planes are, respectively,

$$I_{h0}(x,y,t) = A^2 + |O(x,y,z_h,t)|^2 + 2A\,\mathrm{Re}[O(x,y,z_h,t)], \tag{14}$$

$$\begin{aligned} I_{h\pi/2}(x,y,t) &= A^2 + |O(x,y,z_h,t)|^2 + 2A\,\mathrm{Re}[O(x,y,z_h,t)\mathrm{e}^{-\imath\pi/2}] \\ &= A^2 + |O(x,y,z_h,t)|^2 + 2A\,\mathrm{Im}[O(x,y,z_h,t)]. \end{aligned} \tag{15}$$

The recording of the optical filed intensity on the sensitive medium implies a time-integration over the exposure time T_E of Eqs. (14) and (15) (see e.g., Ref. [14]). In this work, T_E is assumed much smaller than the period of oscillation of the highest harmonics of the motion analyzed,[4] and the medium response is assumed proportional to the identity operator. Thus, the fields recorded are considered proportional to the optical field intensities in Eqs. (14) and (15). Then, since A is known and $|O(x,y,z_h,t)|^2$ can be easily measured, $\mathrm{Re}[O(x,y,z_h)]$ and $\mathrm{Im}[O(x,y,z_h,t)]$ may be evaluated using the above equations.

3.1. Digital reconstruction and displacement field estimate

As shown above, we may obtain the complex optical fields $O_r(x,y,z_h)$ and $O(x,y,z_h,t)$ coming, respectively, from the object at rest and from the vibrating object. Then we may reconstruct the original fields on the object plane via digital simulation of laser light propagation. According to Huygens–Fresnel principle we may write

$$V_r(x,y,z_o) = \int_{-\infty}^{\infty}\int_{-\infty}^{\infty} K^*(x-\xi, y-\eta, z_o - z_h)O_r(\xi,\eta,z_h)\,\mathrm{d}\xi\,\mathrm{d}\eta, \tag{16}$$

$$V(x,y,z_o,t) = \int_{-\infty}^{\infty}\int_{-\infty}^{\infty} K^*(x-\xi, y-\eta, z_o - z_h)O(\xi,\eta,z_h,t)\,\mathrm{d}\xi\,\mathrm{d}\eta, \tag{17}$$

[4]The possibility to satisfy such a condition in practical applications depends on a large number of parameters related to the physical phenomenon and to the characteristics of the experimental rig (e.g., medium sensitivity, laser power, object dimensions, etc.).

where

$$K(x,y,z) = -\frac{\imath e^{ikr}}{\lambda r}\cos\vartheta, \tag{18}$$

where λ is wavelength of the laser light, $r = \|\mathbf{r}\|$ (with $\mathbf{r} = x\mathbf{i} + y\mathbf{j} + z\mathbf{k}$) and ϑ is the angle between $\mathbf{r}$ and the z-axis. Once $V_r(x,y,z_o)$ and $V(x,y,z_o,t)$ are known, $w(x,y,t)$ may be evaluated through Eq. (11).

4. Numerical results

In the present work, the formulation presented is validated through simple applications to the evaluation of the natural modes of vibration of the structure, via the combined use of KLD and holographic interferometry. It should be emphasized that the whole process is digitally simulated, using an in-house developed computer program, including the holographic recording and reconstruction. In this section, we present the results obtained under the assumption that experimental noise is negligible (this assumption is removed in the next section).

For the sake of simplicity, and without loss of generality, we assume that the object dimensions are small with respect to the the distance $d = |z_h - z_o|$ (see Fig. 1), and thus the Fresnel approximation to the optical propagation laws is applicable (for details, see Refs. [17,20]). Furthermore, the response of the recording media is described by the identity operator. We concentrate our analysis on two-dimensional homogeneous structures, whose fundamental modes are known analytically. In connection with these test cases, we examine the influence on the solution of various parameters.

Consider first a vibrating rectangular simply supported uniform plate (with dimensions a and b, thickness h, density ϱ, Young modulus E and Poisson ratio ν), subject to an impulsive force applied at $\mathbf{x} = (x_*, y_*)$ for $t = 0$. The solution to this problem (truncated to $M \times M$ modes) is given by

$$w(x,y,t) = \sum_{m,n=1}^{M} c_{mn}\sin(\omega_{mn}t)\phi_{mn}(x,y), \tag{19}$$

where $\omega_{mn} = \pi^2\sqrt{D/\varrho}(m^2/a^2 + n^2/b^2)$ (with $D = Eh^3/(1-\nu^2)12$) is the natural frequency of the fundamental mode of vibration $\phi_{mn}(x,y)$, given by

$$\phi_{mn}(x,y) = \frac{2}{ab}\sin\left(\frac{m\pi}{a}x\right)\sin\left(\frac{n\pi}{b}y\right), \tag{20}$$

whereas $c_{mn} = \phi_{mn}(x_*, y_*)/\omega_{mn}$.

The optical process is simulated by digitizing the optical fields with a resolution of 9 μm. A mesh of 5440×4080 pixels is processed to obtain the object optical field on the recording plane (see Figs. 2 and 3).[5] Specifically, a truncation order $M = 6$ was assumed, the sampling frequency of the CCD was set to 5×10^{-6} s and the recording time was $T = 0.5$ s (100,000 time samples). [The

[5]The optical simulation is conducted by assuming the recording medium being a Kodak full-frame CCD image sensor KAF-22000CE, with an array of 5440×4080, 9 μm square pixels.

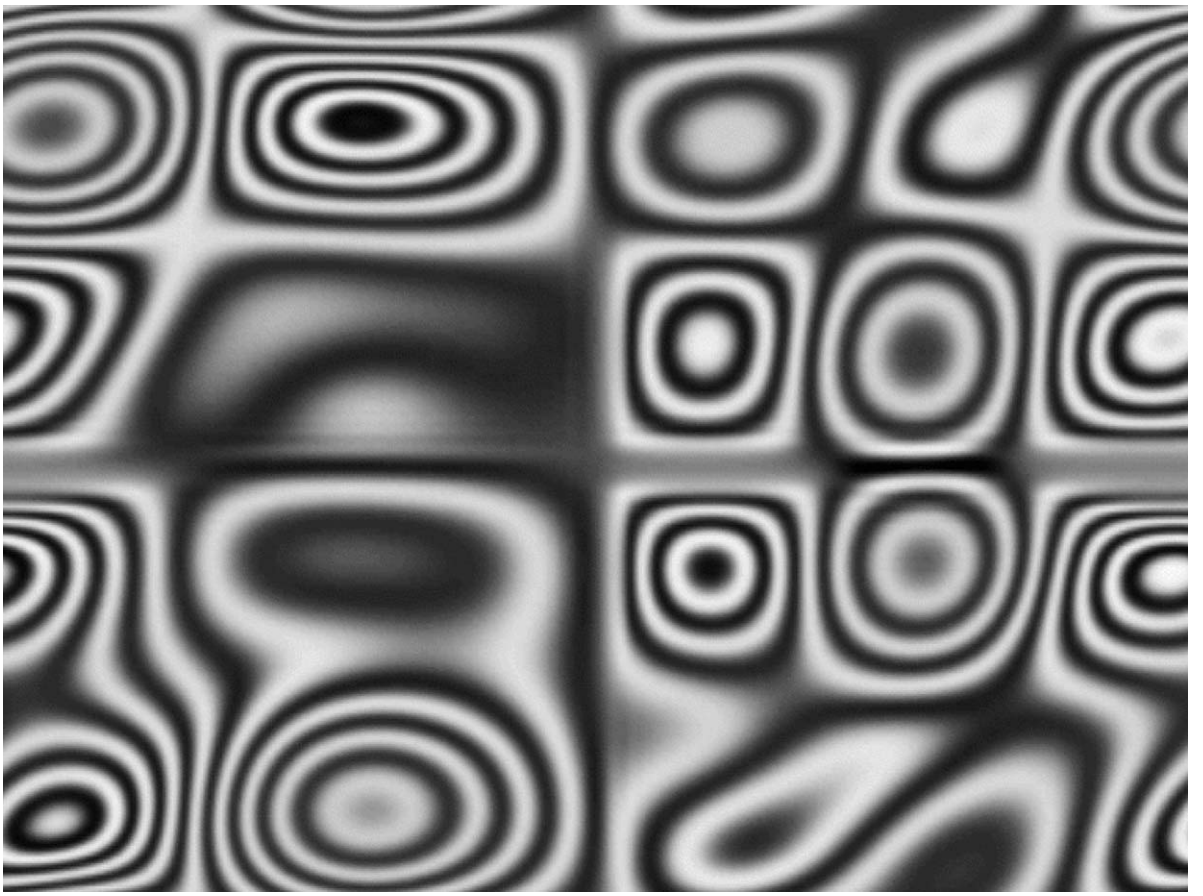

Fig. 2. Density plot of the real part of $O(x, y, z_h, \hat{t})$ for the rectangular simply supported plate at $\hat{t} = 0.05$ s.

effect of the recording time is related to the use of the time-averaged autocorrelation of the displacements in the KLD technique. Specifically, it is necessary to provide to the average operator a recording time sufficiently long, so as to have a significant number of oscillation periods also for the lower harmonics. In other words, the number of available time samples must be sufficiently high so as to provide a data ensemble capable of representing the dynamics of all the harmonics.] The displacement field is calculated from the phase shift between the two optical fields and is stored in a 40×30 mesh to be processed using the KLD (Figs. 4–6). Fig. 7 presents the reconstructed displacement field along the $x = a/2$ cut of the plate; this is compared to its analytical representation. Moreover, the Karhunen–Loève eigenvalues (KLV's) are shown in Fig. 8 and some of the Karhunen–Loève modes (KLM's) are presented in Figs. 9–12. It is worth noting that, having used $M = 6$, only the first 36 KLV's and KLM's are physically meaningful (see Eq. (19)). The remaining eigenvalues represent the noise tail (due to round-off error, in this case) of the decomposed field and the corresponding eigenfunctions are physically meaningless. Finally, the method used by Wolter [11] has been utilized for finding the natural frequencies corresponding to the modes obtained. Specifically, the time-history of the displacement field has

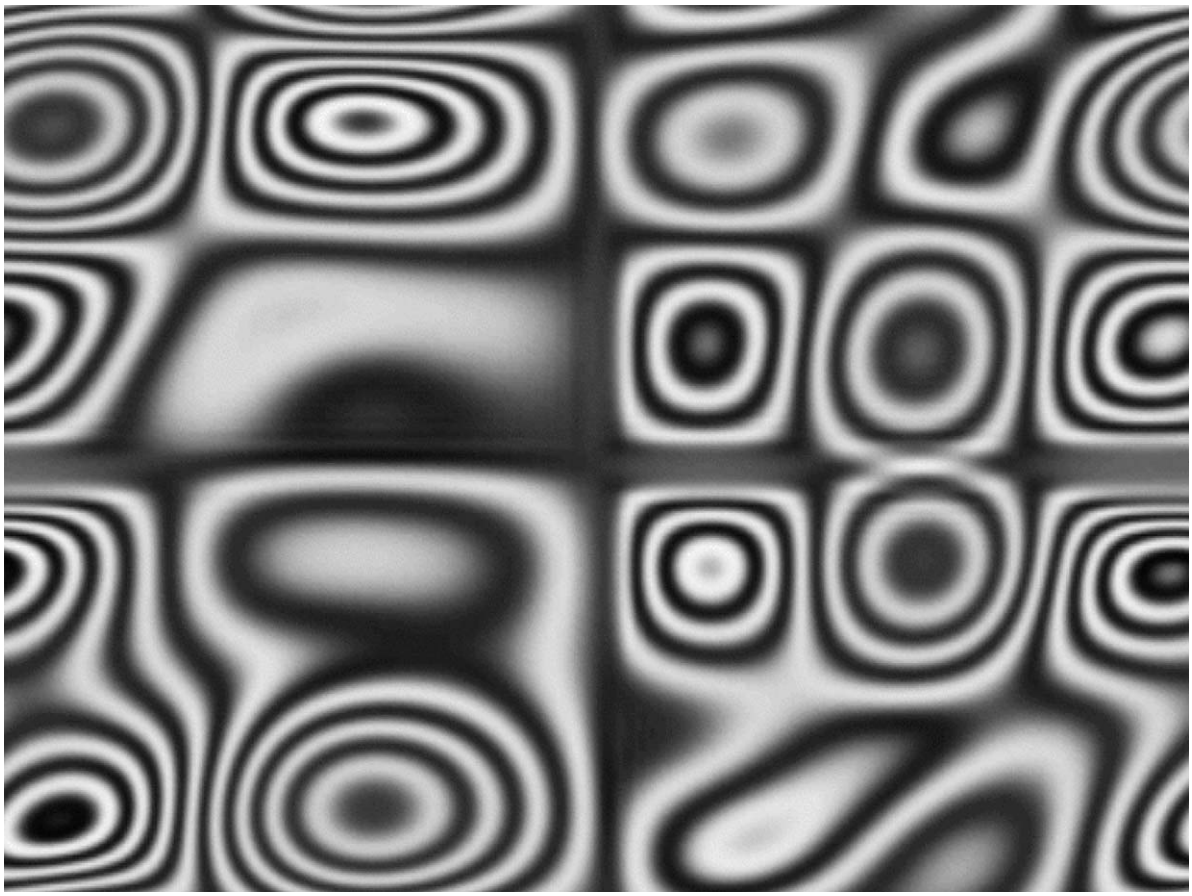

Fig. 3. Density plot of the imaginary part of $O(x, y, z_h, t)$ for the rectangular simply supported plate at $t = 0.05$ s.

been projected on each KLM and the resulting signal has been Fourier transformed. The results are presented in Fig. 13 for KLM $\phi_{6,2}$. The peak occurs at 22,412 Hz and this is considered as the frequency provided by the method. This is in remarkable agreement with the analytical value, which is 22,411 Hz.

Next, consider a uniform cantilever plate. We consider only the bending deformation of the plate, so that the vertical displacement corresponds to that of a cantilever beam. Thus,

$$w(x, y, t) = \sum_{k=1}^{M} c_k \sin(\omega_k t)\phi_k(x, y), \tag{21}$$

where $\omega_k = \sqrt{(D/\rho)}\eta_k^2$, with η_k being the solutions of the characteristic equation $\cos \eta_k \cosh \eta_k = -1$, and

$$\phi_k(x, y) = A_k\left[\sin\left(\eta_k \frac{x}{a}\right) - \sinh\left(\eta_k \frac{x}{a}\right)\right] + B_k\left[\cos\left(\eta_k \frac{x}{a}\right) - \cosh\left(\eta_k \frac{x}{a}\right)\right], \tag{22}$$

whereas $c_k = \phi_k(x_*, y_*)/\omega_k$.

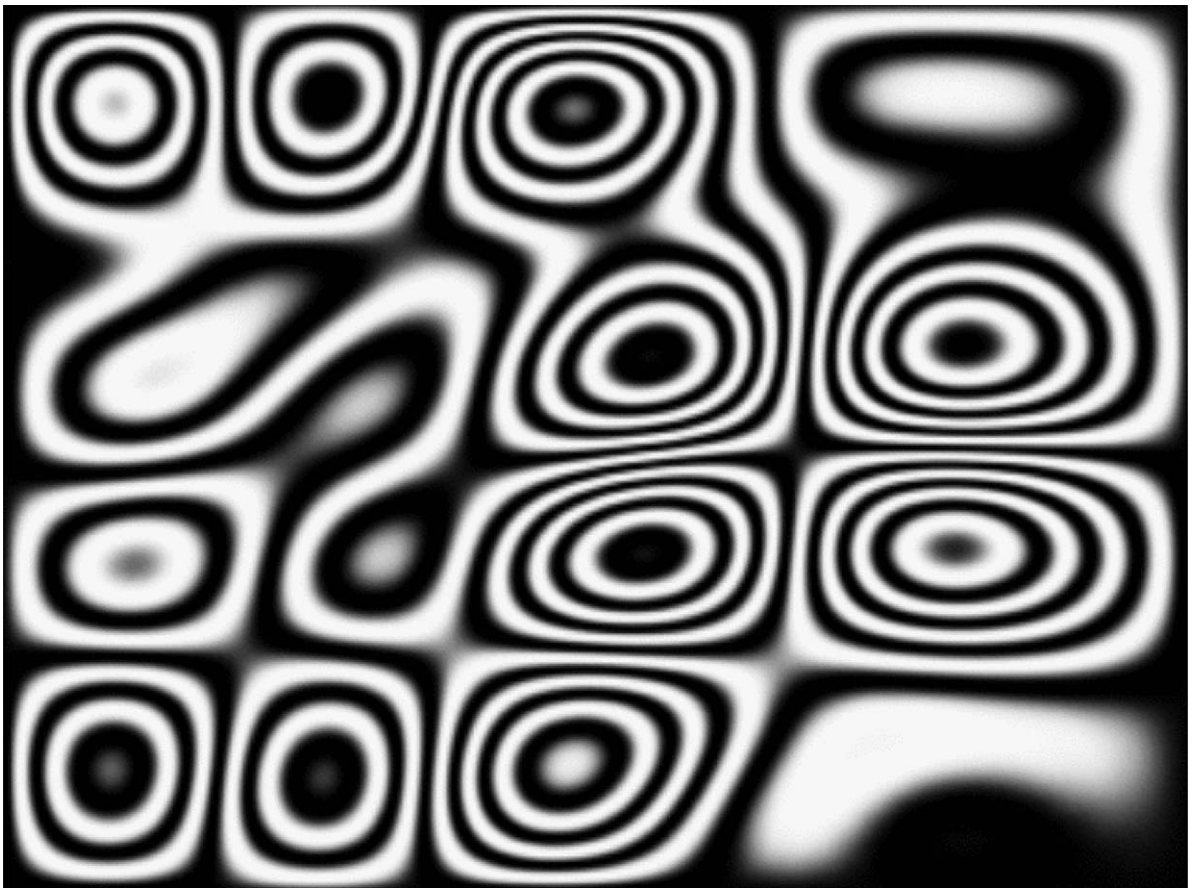

Fig. 4. Density plot of the real part of $V_r(x, y, z_o, t)$ for the rectangular simply supported plate at $t = 0.05$ s.

The truncation order was taken as $M = 10$ and $N = 10,000$ was the number of available time samples, with $T = 0.05$ s. The whole analysis process was performed as above. The results are presented in Figs. 14–22. Figs. 14–20 are similar to those for the simply supported plate and need no further explanation. Fig. 21 presents a cross-section of Fig. 20. In addition, the figure presents (for the same problem and still using a number of processed time samples $N = 10,000$), the results obtained by using (instead of constant recording time steps that satisfy the sampling theorem) random time steps with a mean value of 0.1 s (so that $T = 1000$ s). In addition, the results are compared with the analytical ones; again the agreement is very good, especially if we take into account the high order of the mode. It should also be noted that the agreement between the uniform-sampling and random-sampling results is also very good, indicating that it is possible to perform the KLD analysis without satisfying Shannon's time-sampling theorem. Obviously this would not be acceptable if, in addition, the natural frequencies were to be required. It may be added that, since the KLD is a statistical method, the number of time samples available (rather than time-sampling frequency), along with the number of spatial samples, are the relevant

Fig. 5. Density plot of the imaginary part of $V_r(x, y, z_o, t)$ for the rectangular simply supported plate at $t = 0.05$ s.

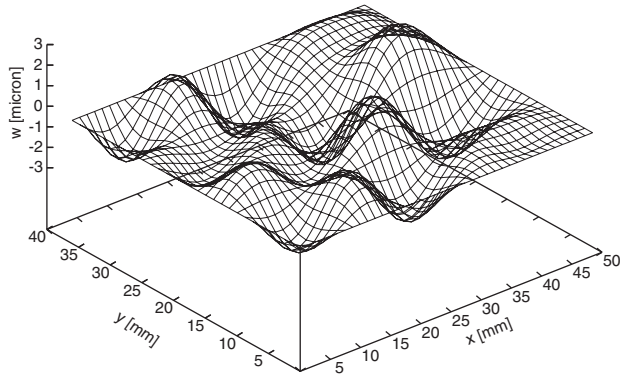

Fig. 6. Displacements, evaluated from the optical-field phase shift at $t = 0.05$ s.

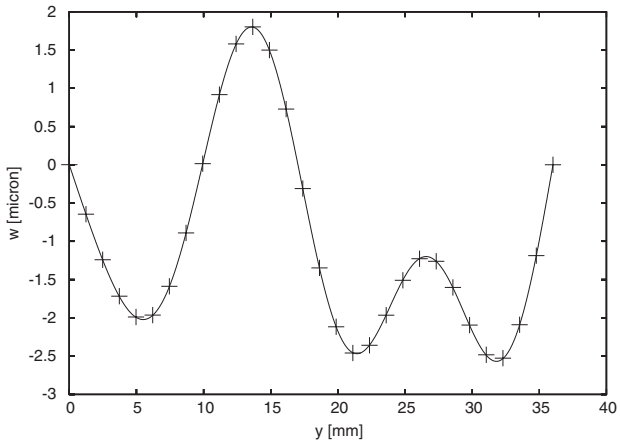

Fig. 7. Comparison between analytical (——) and extracted (+) displacements at $x = a/2$, for $t = 0.05$ s.

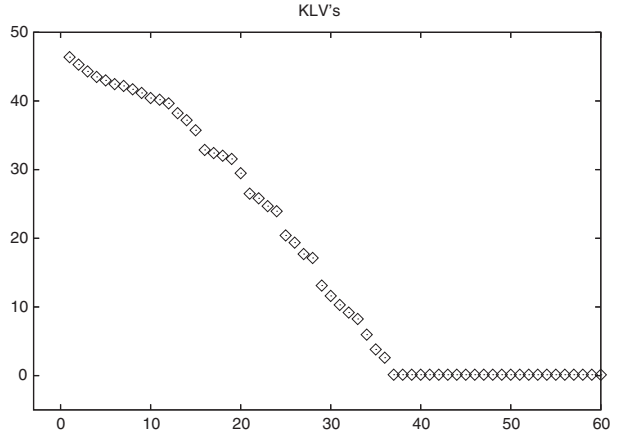

Fig. 8. First 60 KLD eigenvalues.

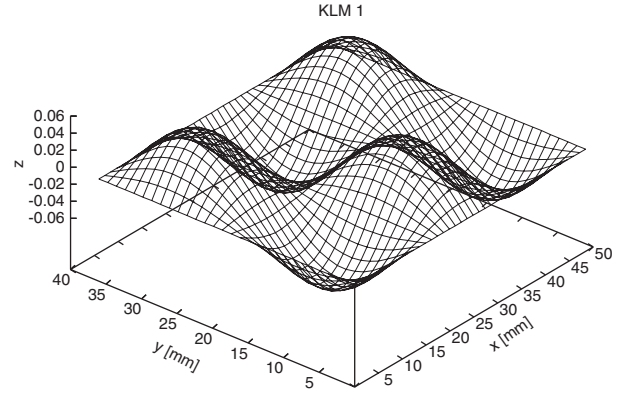

Fig. 9. First Karhunen–Loève mode ($\phi_{3,2}$).

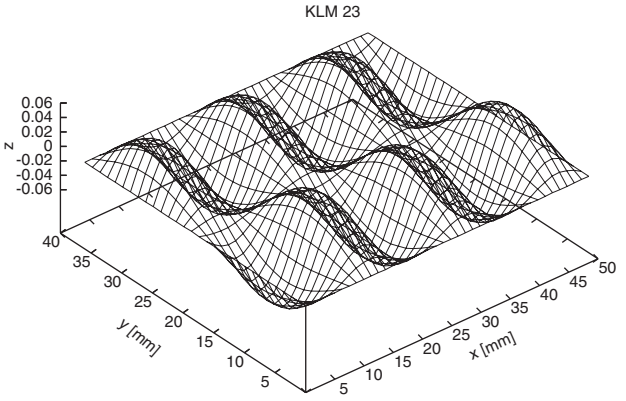

Fig. 10. 23rd Karhunen–Loève mode ($\phi_{6,2}$).

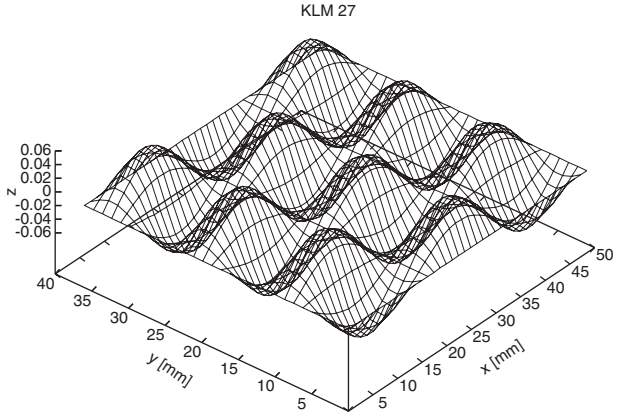

Fig. 11. 27th Karhunen–Loève mode ($\phi_{3,6}$).

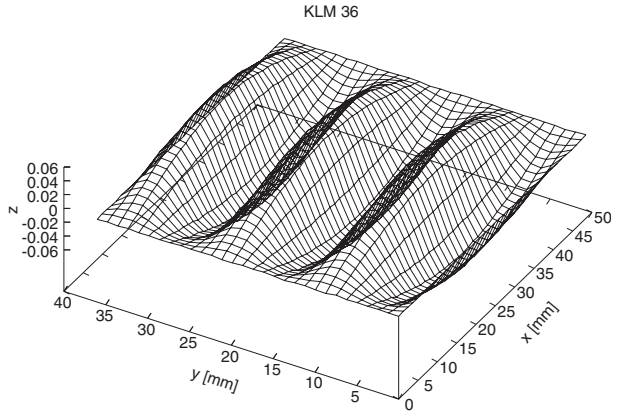

Fig. 12. 36th Karhunen–Loève mode ($\phi_{1,6}$).

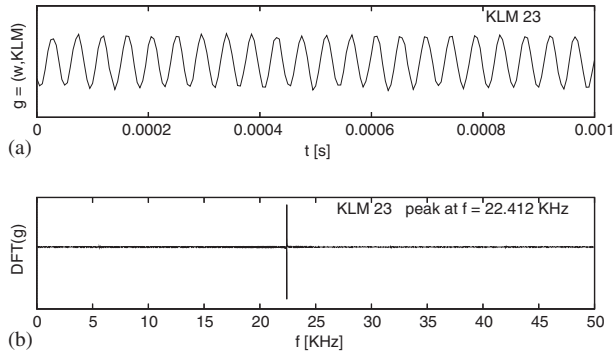

Fig. 13. Projection of the displacement distribution field onto 23rd Karhunen–Loève mode ($\phi_{6,2}$): (a) time domain and (b) frequency domain.

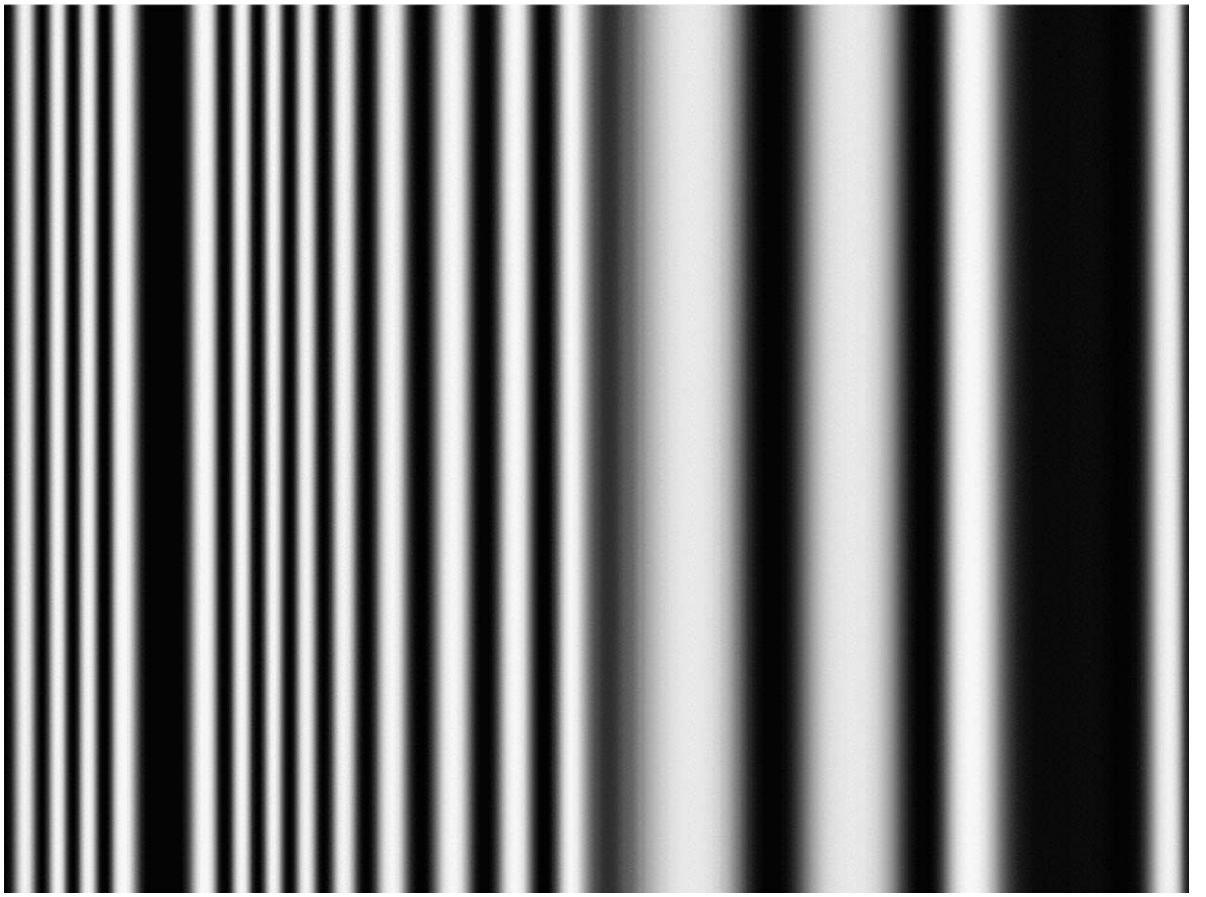

Fig. 14. Density plot of the real part of $O(x, y, z_h, t)$ for the rectangular cantilever plate at $t = 0.03$ s.

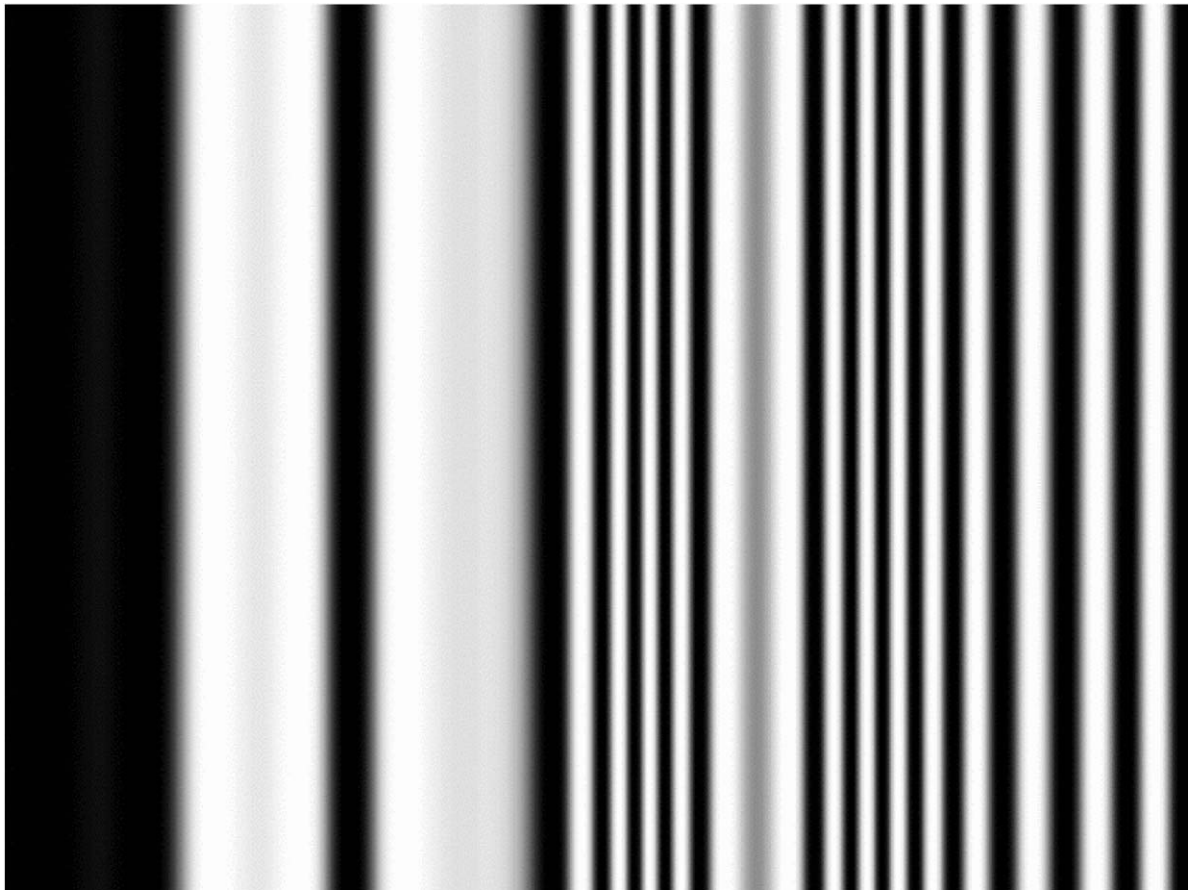

Fig. 15. Density plot of the imaginary part of $O(x, y, z_h, t)$ for the rectangular cantilever plate at $t = 0.03$ s.

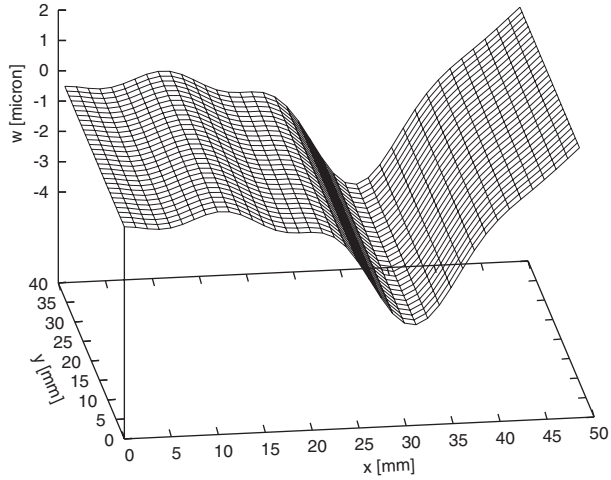

Fig. 16. Displacements evaluated from the optical-field phase shift at $t = 0.03$ s.

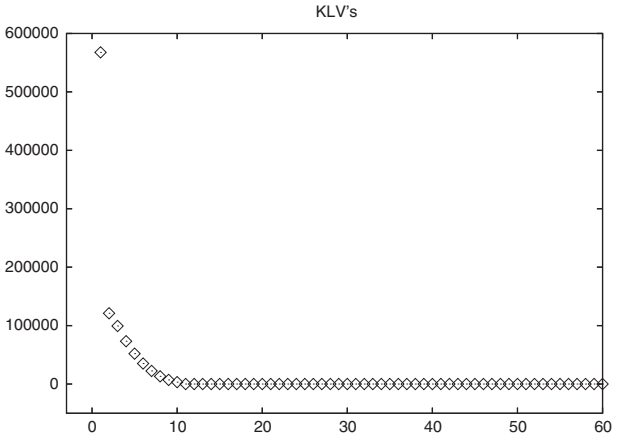

Fig. 17. First 60 KLD eigenvalues.

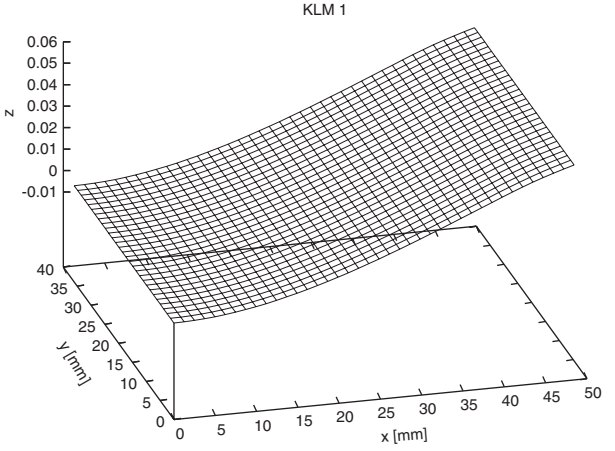

Fig. 18. First Karhunen–Loève mode (ϕ_1).

parameters for modal identification. Fig. 22 shows the rms of the error made in the identification of modal shapes. Specifically, the figure depicts the error $e_k = [1/2 \int (\varphi_k - \phi_k)^2 \, d\mathbf{x}]^{1/2}$ as a function of the mode number k, when a displacement field that includes 50 modes is processed over a mesh of 40×30 points. Since (contrary to the time sampling) the spatial sampling has to fulfill Shannon's theorem, the spatial resolution represents a limit for capturing high-order (and high-frequency) modal shapes. It should be noted that, as expected, the numerical methodology used introduces spurious solutions (due to a violation of Shannon's sampling theorem in space). In this case the eigensolutions have nothing to do with the analytical modes. As shown in Fig. 22, after a certain point $e_k = 1$. This implies that the two functions φ_k and ϕ_k are such that $\int \varphi_k \phi_k \, d\mathbf{x} = 0$ (see Appendix B). Note that the transition is quite sudden.

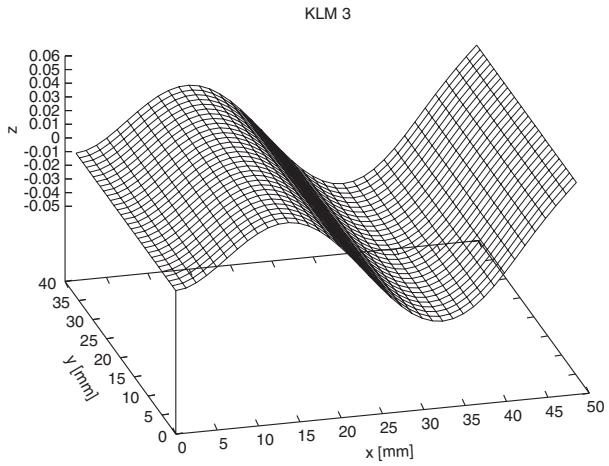

Fig. 19. Third Karhunen–Loève mode (ϕ_3).

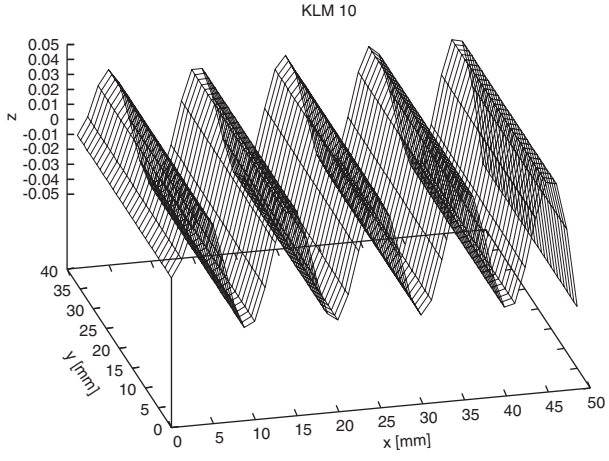

Fig. 20. Tenth Karhunen–Loève mode (ϕ_{10}).

It has been shown that $\varphi_k(\mathbf{x}) = \phi_k(\mathbf{x})$. It follows that the fundamental modes of vibration represent the optimal basis functions in the energy content sense. It is worth noting that Eq. (21) states that $w(\mathbf{x}, t)$ is a quasi-periodic function of time, not necessarily a periodic function. This is important because, in general, the natural-frequency ratios are not rational.

5. Effects of experimental noise

One could argue that the results presented above are not really significant, because of the absence of (simulated) experimental noise. Indeed, whatever test rig and instrumentation are used

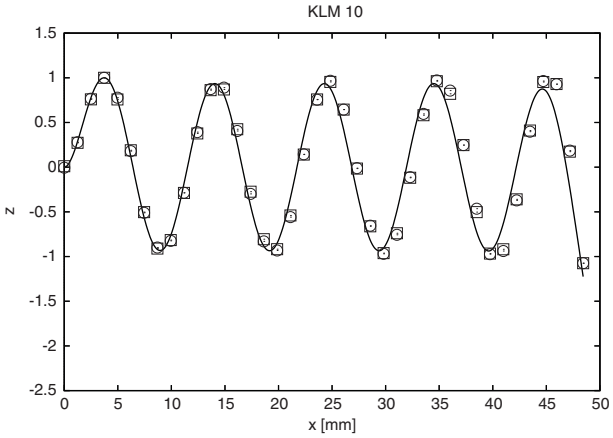

Fig. 21. Comparison between the 10th Karhunen–Loève mode obtained, respectively, with a uniform time-sampling (□) and with a random time-sampling (○), and the corresponding analytical mode at $y = b/2$.

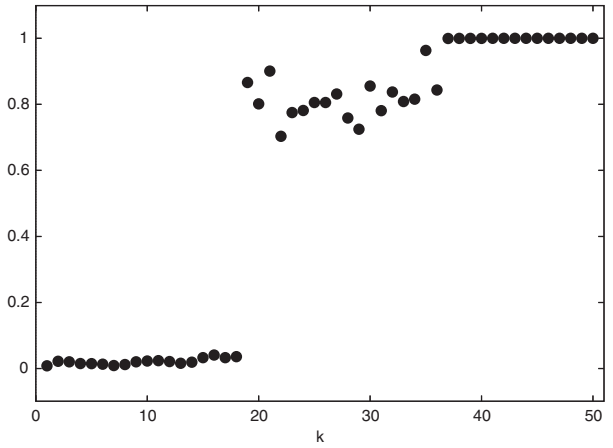

Fig. 22. The rms of error in modal identification mode number k.

to generate and record the signal, the presence of unwanted noise is unavoidable. In real-life applications, experimental noise is always present in the input of the Karhunen–Loève algorithm. Hence, in this subsection, we investigate on the effects of the experimental noise on the identification of modal shapes.

Specifically, we assume that the signal processed by the KLD is $\hat{w}(\mathbf{x}_i, t) = w(\mathbf{x}_i, t) + \eta(\mathbf{x}_i, t)$, where $\eta(\mathbf{x}_i, t)$ is the generic experimental noise evaluated at $\mathbf{x} = \mathbf{x}_i$. In order to formulate this, it is convenient to discuss the discretized form of the eigenproblem integral equation, (Eq. (1)). In this work, the discretization is obtained by dividing the surface $\mathscr{S}$ into small elements $\mathscr{S}_i$, and assuming the integrand to be constant within each element, and equal to its value at the center $\mathbf{x}_i$

of the element $\mathscr{S}_i$ (we use the symbol $\psi_i \coloneqq \varphi(\mathbf{x}_i)$ in order to avoid confusion with the eigenfunctions φ_i). This yields

$$\sum_j \hat{r}_{ij}\psi_j \mathscr{S}_j = \lambda\psi_i, \tag{23}$$

where

$$\hat{r}_{ij} = \frac{1}{N}\sum_{k=0}^{N} \hat{w}(\mathbf{x}_i, t_k)\hat{w}(\mathbf{x}_j, t_k). \tag{24}$$

The elements of the autocorrelation matrix $\hat{\mathbf{R}} \coloneqq [\hat{r}_{ij}]$ may be expressed as

$$\hat{r}_{ij} = r_{ij} + p_{ij} + p_{ji} + q_{ij}, \tag{25}$$

where

$$r_{ij} \coloneqq \frac{1}{N}\sum_{k=0}^{N} w(\mathbf{x}_i, t_k)w(\mathbf{x}_j, t_k), \tag{26}$$

$$p_{ij} \coloneqq \frac{1}{N}\sum_{k=0}^{N} w(\mathbf{x}_i, t_k)\eta(\mathbf{x}_j, t_k), \tag{27}$$

$$q_{ij} \coloneqq \frac{1}{N}\sum_{k=0}^{N} \eta(\mathbf{x}_i, t_k)\eta(\mathbf{x}_j, t_k). \tag{28}$$

It is apparent that, if $w(\mathbf{x}_i, t)$ and $\eta(\mathbf{x}_j, t)$ are uncorrelated for all i and j, then (in the $N \to \infty$ limit) p_{ij} vanishes. If, in addition, $\eta(\mathbf{x}_i)$ and $\eta(\mathbf{x}_j)$ are uncorrelated for $i \neq j$, then (again in the $N \to \infty$ limit) q_{ij} vanishes for $i \neq j$. As a result, we obtain $\hat{r}_{ij} = r_{ij} + \overline{\eta_i^2}\delta_{ij}$, where $\overline{\eta_i^2} = (1/N)\sum_k \eta^2(\mathbf{x}_i, t_k)$. In the following, for the sake of simplicity, we assume that the level of noise is spacially uniform, independently of the local level of the signal. This implies that the noise is independent of i; therefore, $(1/N)\sum_k \eta^2(\mathbf{x}_i, t_k) = \text{constant} = \overline{\eta^2}, \forall \mathbf{x}_i$. Thus,

$$\hat{\mathbf{R}} = \mathbf{R} + \overline{\eta^2}\mathbf{I}. \tag{29}$$

It is apparent that the matrices $\hat{\mathbf{R}}$ and $\mathbf{R} \coloneqq [r_{ij}]$ have the same set of eigenvectors and, moreover, the corresponding eigenvalues are given by

$$\hat{\lambda}_k = \lambda_k + \overline{\eta^2}. \tag{30}$$

We can summarize our results by stating that, whenever Eq. (29) holds (i.e., whenever (1) the noise and the signal are uncorrelated, (2) the noise signals at two points are uncorrelated, and (3) the level of noise is spacially uniform), the experimental noise does not affect the modal shapes. It is worth noting that, in actual applications, having a large number N of time samples available is crucial for: (1) the convergence of the time-averaged autocorrelation function to the form expressed by Eq. (8), and (2) for the convergence of the experimental noise to a contribution expressed by Eq. (29). In other words, the data ensemble processed by the method, has to be "statistically representative" of the dynamic phenomenon.

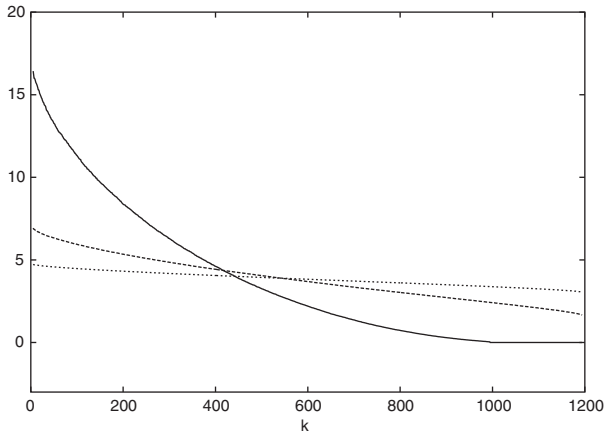

Fig. 23. $\hat{\lambda}_k - \lambda_k$ versus mode number k for a number of time samples available $N = 1000$ (——), $N = 10,000$ (- - -) and $N = 100,000$ ($\cdots$), and with a signal-to-noise ratio equal to 0.1.

The above formulation has been applied to both simply supported and cantilever plates. For all the numerical results obtained, a random noise with a signal-to-noise ratio[6] $s/n = 0.1$ has been added to the KLD input (i.e., to the displacement field reconstructed from the digital holograms) and the modal analysis have been performed as described above. The modal shapes thus obtained coincide, within plotting accuracy, with those presented in Section 4, and therefore are not reproduced here.

Thus, in the following we concentrate on noise-related issues, specifically on whether the eigenvalues satisfy Eq. (30). Fig. 23 depicts $\hat{\lambda}_k - \lambda_k$ as a function of k, for different numbers of available time samples N and $s/n = 0.1$ (of course, most of the λ's equal zero, because the corresponding modal shapes do not appear in the signal). It may be observed that, as N grows, the curve tends to a horizontal line (as it should, since according to Eq. (30), the limit is $\overline{\eta^2}$, which is constant). It may be noted that the results, still for $N = 10,000$, were repeated for signal-to-noise ratios $s/n = 0.01, 0.02, 0.05, 0.1$: the results for $\hat{\lambda}_k - \lambda_k$ as a function of k are virtually identical, except of course for a multiplicative constant equal to $(s/n)^2$ (and hence are not shown here explicitly). Finally, Fig. 24 presents an example of the convergence of the experimental noise. Specifically, Fig. 24 depicts $\|\mathbf{P}\|/\|\hat{\mathbf{R}}\|$ and $\|\mathbf{Q}\|/\|\hat{\mathbf{R}}\|$ as a function of $1/N$, where $\mathbf{P} := [p_{ij} + p_{ji}]$, $\mathbf{Q} := [q_{ij} - q_{ii}\delta_{ij}]$ (no sum over repeated indices is implied), and $\|\mathbf{A}\| = \sqrt{\mathrm{tr}(\mathbf{A}^{\mathrm{T}}\mathbf{A})}$ is the Frobenius norm of the matrix $\mathbf{A}$.

6. Concluding remarks

A non-invasive methodology for the evaluation of the natural modes of vibration has been presented. Specifically, the formulation, based on a combination of the KLD technique with the

[6]The value of the signal is calculated as the peak value of $w(\mathbf{x}, t)$.

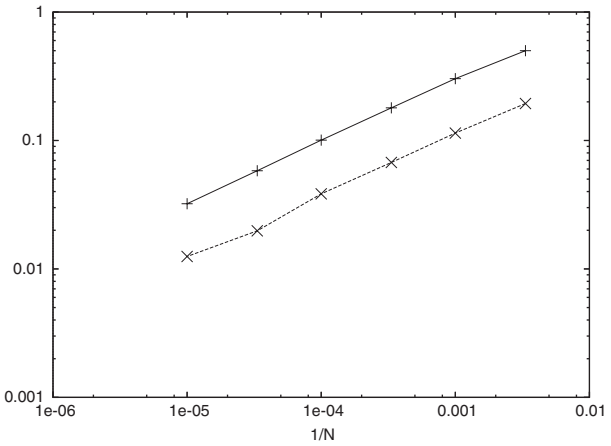

Fig. 24. Example of noise convergence: $\|\mathbf{Q}\|/\|\hat{\mathbf{R}}\|$ (+) and $\|\mathbf{P}\|/\|\hat{\mathbf{R}}\|$ (×).

holographic analysis, is aimed at the experimental evaluation of the fundamental modes of vibration of oscillating two-dimensional structures that have constant mass per unit area. The elastic displacements of the structure under investigation are obtained by post-processing a sequence of holograms of the vibrating object. The KLD is then applied to the displacement field to extract the empirical base functions. These represent the basis that, for a given truncation order n, retains on average the maximum energy content. The coupling of these two techniques appears to have several interesting features, resulting in the possibility of an accurate analysis of vibrating objects with a relatively inexpensive experimental rig. The equivalence of the KLD empirical base functions to the eigenfunctions of the structural operator has been shown for structures that have constant mass per unit area. The method has been preliminarily assessed by simulating the optical process with a computer code. The dynamics of simple structures has been generated analytically and processed with the method presented. The process simulated consists in recording (and then digitally reconstructing) two series of a (sufficiently) large number of holograms. The displacement field is calculated from optical field phase shift and then down-sampled to be decomposed through the KLD. In this work, a large number of holograms has been used (100,000 in the first example presented and 10,000 in the second one). The structure has been assumed undamped. In real acquisitions, the presence of damping limits the observation time and, thus, some technique (e.g., excitation with a train of impulsive forces) has to be used to sustain the vibration.

The results presented here reveal that the KLD modes are in excellent agreement with the fundamental modes of the structure, confirming that, for distinct frequencies, $\varphi_k(\mathbf{x}) = \phi_k(\mathbf{x})$. Issues related to the experimental noise, always present in practical applications, have been also addressed. Their effects have been taken into account in the simulation process, demonstrating that the modes extracted are not influenced by noise with spacially uniform amplitude, as long as this is uncorrelated.

Finally, a preliminary study was performed to address what happens when two frequencies coalesce and the results are presented in Figs. 25 and 26, which depict the KLMs $\phi_{1,2}$ and $\phi_{2,1}$ of a

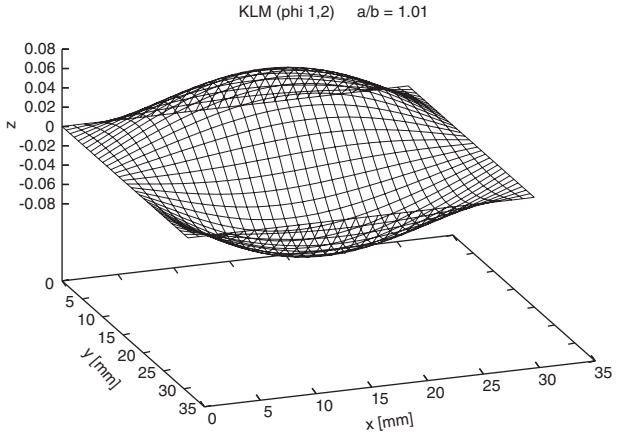

Fig. 25. Modal identification for nearly square plates. Karhunen–Loève mode $\phi_{1,2}$.

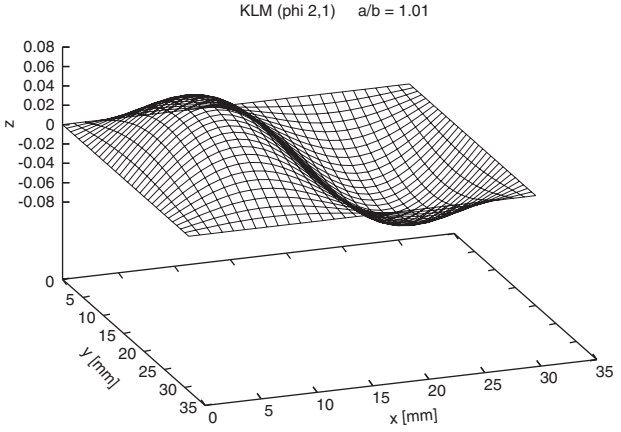

Fig. 26. Modal identification for nearly square plates. Karhunen–Loève mode $\phi_{2,1}$.

nearly square simply supported plate for which the edge-ratio is 1.01. In this case, it is apparent that the modal shapes are distinct and it may be shown that they are in excellent agreement with the analytical modes. The issues related to the modal identification of structures for which $\omega_i = \omega_k$ (for some i, k) warrant further evaluation and will be the subject of future work. In addition, an extension of the KLD to the analysis of three-dimensional structures with non-constant density is currently under development.

Acknowledgments

The authors wish to thank Prof. Jerome H. Milgram of the Massachusetts Institute of Technology, for introducing them to the wondrous enchanted world of digital holography.

Appendix A. Diagonality of the matrix C

Here, we want to prove what stated by Eq. (7). The coefficients of the matrix **C** are by definition

$$c_{ik} \coloneqq \frac{1}{T}\int_0^T \alpha_i(t)\alpha_k(t)\,\mathrm{d}t, \tag{31}$$

where the product $\alpha_i\alpha_k$ is given by (see Eq. (4))

$$\begin{aligned}\alpha_i(t)\alpha_k(t) &= \tfrac{1}{4}a_i a_k[\mathrm{e}^{\imath(\omega_i t+\chi_i)} + \mathrm{e}^{-\imath(\omega_i t+\chi_i)}][\mathrm{e}^{\imath(\omega_k t+\chi_k)} + \mathrm{e}^{-\imath(\omega_k t+\chi_k)}]\,\mathrm{d}t\\ &= \tfrac{1}{4}a_i a_k\{\mathrm{e}^{\imath[(\omega_i+\omega_k)t+(\chi_i+\chi_k)]} + \mathrm{e}^{-\imath[(\omega_i+\omega_k)t+(\chi_i+\chi_k)]}\}\\ &\quad + \tfrac{1}{4}a_i a_k\{\mathrm{e}^{\imath[(\omega_i-\omega_k)t+(\chi_i-\chi_k)]} + \mathrm{e}^{-\imath[(\omega_i-\omega_k)t+(\chi_i-\chi_k)]}\}.\end{aligned} \tag{32}$$

Under the condition that $\omega_i \neq \omega_k$ for $i \neq k$, it is apparent that

$$\lim_{T\to\infty} c_{ik} = \tfrac{1}{2}a_k^2\delta_{ik}. \tag{33}$$

Appendix B. Root mean square of the error in modal identification

In order to evaluate the error made in the identification of modal shapes, we utilized its rms value, defined as

$$e_k = \sqrt{\frac{1}{2}\int_{\mathscr{S}}[\phi_k(\mathbf{x}) - \varphi_k(\mathbf{x})]^2\,\mathrm{d}\mathbf{x}}, \tag{34}$$

where the analytical modes and the Karhunen–Loève eigenfunctions are normalized so as

$$\int_{\mathscr{S}} \phi^2(\mathbf{x})\,\mathrm{d}\mathbf{x} = 1, \quad \int_{\mathscr{S}} \varphi^2(\mathbf{x})\,\mathrm{d}\mathbf{x} = 1. \tag{35}$$

Eq. (34) may be written as

$$e_k = \frac{1}{\sqrt{2}}\sqrt{\int_{\mathscr{S}} \phi_k^2(\mathbf{x})\,\mathrm{d}\mathbf{x} + \int_{\mathscr{S}} \varphi_k^2(\mathbf{x})\,\mathrm{d}\mathbf{x} - 2\int_{\mathscr{S}} \phi_k(\mathbf{x})\varphi_k(\mathbf{x})\,\mathrm{d}\mathbf{x}}. \tag{36}$$

It is apparent that if (and only if) $\int_{\mathscr{S}} \phi_k\varphi_k\,\mathrm{d}\mathbf{x} = 0$, then $e_k = 1$ (see the equation above). Note that, in this case, the corresponding KLM's have no physical meaning and thus the KLD is unable to identify the related modal shapes.

References

[1] H. Hotelling, Analysis of a complex of statistical variables into principal components, *Journal of Educational Psychology* 24 (1933) 417–441 and 498–520.
[2] D. Kosambi, Statistics in function space, *Journal of Industrial Mathematical Society* 7 (1943) 76–88.
[3] M. Loéve, Fonctions aléatoire de second ordre, *Compte Rendus des Academie des Sciences* 220 (1945).

[4] K. Karhunen, Zur Spektraltheorie stokastisher Prozesse, *Annales Academiae Scientiorum Fennicae, Series A* 1 (1946).
[5] J.L. Lumley, The structure of inhomogeneous turbulence, in: A.M. Yaglom, V.I. Tatarsky (Eds.), *Atmospheric Turbulence and Wave Propagation*, Nauka, Moscow, 1967, pp. 166–178.
[6] P. Holmes, J.L. Lumley, G. Berkooz, *Turbulence, Coherent Structures, Dynamical Systems and Symmetry*, Cambridge University Press, Cambridge, 1996.
[7] B.F. Feeny, R. Kappagantu, On the physical interpretation of proper orthogonal modes in vibrations, *Journal of Sound and Vibration* 211 (1998) 607–616.
[8] B.F. Feeny, On proper orthogonal coordinates as indicators of modal activity, *Journal of Sound and Vibration* 255 (2002) 805–817.
[9] B.F. Feeny, On the proper orthogonal modes and normal modes of continuous vibration systems, *Journal of Vibration and Acoustics* 124 (2002) 157–160.
[10] G. Kerschen, J.C. Golinval, Physical interpretation of the proper orthogonal modes using the singular value decomposition, *Journal of Sound and Vibration* 249 (2002) 849–865.
[11] C. Wolter, M.A. Trinidade, R. Sampaio, Obtaining mode shapes through the Karhunen–Loève expansion for distributed-parameter linear systems, *Shock and Vibration* 9 (2002) 177–192.
[12] C. Wolter, R. Sampaio, Comparison between the use of Karhunen–Loève expansion and mode shapes in the model reduction of linear systems, in: J.J. Espíndola, E.M.O. Lopes, F.S.V. Bázan (Eds.), *Dynamic Problems of Mechanics (IX Dname)*, Brazilian Society of Mechanical Sciences (ABCM), Florianópolis, Brazil, March 2001, pp. 453–458.
[13] R.K. Erf, *Holographic Nondestructive Testing*, Academic Press, New York, 1974.
[14] P. Hariharan, *Optical Holography: Principles, Techniques and Applications*, Cambridge University Press, Cambridge, 1984.
[15] C. Wagner, S. Seebacher, W. Osten, W. Jüptner, Digital recording and numerical reconstruction of lensless Fourier holograms in optical metrology, *Applied Optics* 38 (1999) 4812–4820.
[16] L. Xu, X. Peng, J. Miao, A.K. Asundi, Studies of digital microscopic holography with applications to microstructure testing, *Applied Optics* 40 (2001) 5046–5051.
[17] P. Hariharan, B.F. Oreb, N. Brown, Real-time holographic interferometry: a microcomputer system for the measurement of vector displacements, *Applied Optics* 22 (1983) 876–880.
[18] H. Hochstadt, *Integral Equations*, Wiley Classics Library, Wiley, New York, 1973.
[19] J.L. Lumley, *Stochastic Tools in Turbulence*, Academic Press, New York, 1970.
[20] J.H. Milgram, W. Li, Computational reconstruction of images from holograms, *Applied Optics* 41 (2002) 833–864.